

Supporting information

Self-assembly of Janus Au:Fe₃O₄ branched nanoparticles. From organized clusters to stimuli-responsive nanogels suprastructures

Javier Reguera,^{a,b,*} Tatjana Flora,^{c,d} Naomi Winckelmans,^e José C. Rodríguez-Cabello,^{c,d} Sara Bals^e

^a BCMaterials, Basque Center for Materials, Applications and Nanostructures, UPV/EHU Science Park, 48940 Leioa, Spain

^b Ikerbasque, Basque Foundation for Science, 48013 Bilbao, Spain

^c BIOFORGE Lab, University of Valladolid, Edificio Lucia, Paseo de Belén 19, 47011 Valladolid, Spain

^d Biomedical Research Networking Center in Bioengineering Biomaterials and Nanomedicine, Ciber-BBN, Spain

^e EMAT – University of Antwerp, Groenenborgerlaan 171, B-2020 Antwerp, Belgium

Index:

1. Experimental methods	2
a. Chemicals	2
b. Synthesis of catechol-terminated PEG	2
c. Synthesis of thermo-responsive ELR	3
d. Synthesis of Janus Au:Fe ₃ O ₄ nanoparticles	3
e. Amphiphilic functionalization	5
f. Amphiphilic self-assembly	5
g. Thermo-responsive functionalization	6
h. TEM	6
i. ICP	7
j. DLS	8
2. Supporting figures	8
Figure S.1: TEM images of Janus nanoparticles	8
Figure S.2: UV-Vis of the amphiphilic functionalization	9
Figure S.3: UV-Vis of assemblies produced by H ₂ O addition	9
Figure S.4: TEM images of nanoamphiphile assemblies with big nanostars and long hydrophobic polymer	10
Figure S.5 MALDI-TOF spectra of C ₃ (VPGVG) ₈₄ -ELR	10
Figure S.6 DSC graph of C ₃ (VPGVG) ₈₄ -ELR	11
Figure S.7: DLS and UV-Vis of Janus nanoparticles after thermo- responsive functionalization. DLS of only ELR	11

Figure S.8: DLS and SEM of an ELR solution (without stabilizing nanoparticles)	12
Figure S.9: Cryo-TEM of assemblies of thermo-responsive Janus nanoparticles	12
Figure S.10: Light-triggered self-assembly. Heating profile and reversibility	13
3. Supporting Tables	13
Table S.1 Amino acid composition of C ₃ (VPGVG) ₈₄ -ELR	13
4. References	14

1. Experimental methods

a. Chemicals

All chemicals were used as purchased without further purification: hydrogen tetrachloroaurate(III) trihydrate (99.99%, Alfa Aesar), oleylamine (80–90%, Acros Organics), 1-octadecene (90%, Aldrich), oleic acid (90%, Aldrich), iron(0) pentacarbonyl (99.99%, Aldrich), 1,2-hexadecanediol (90%, Aldrich), Dopamine hydrochloride (Aldrich), methoxy-polyethylene glycol acetic acid ($\geq 80\%$, $M_n = 5000 \text{ g mol}^{-1}$), polyvinylpyrrolidone ($M_n = 10000 \text{ g mol}^{-1}$, Aldrich), Thiol-terminated polystyrene ($M_n=2000$ and $M_w=2300 \text{ g/mol}$, and $M_n=20000$ and $M_w=21500$, Polymer Source, Inc.), additional solvents were reagent grade from Aldrich.

b. Synthesis of catechol-terminated PEG

Catechol-terminated PEG was synthesized as previously reported.^[S1] A solution of methoxypolyethylene glycol acetic acid ($\geq 80\%$, $M_n = 5000 \text{ g mol}^{-1}$) (0.5g), EDC (0.11 g), and NHS (6.5 mg) in 10 mL water was stirred at 0°C for 5 min. 0.12 g of dopamine hydrochloride was added to this solution. The mixture was bubbled with N₂ and stirred at

room temperature for 15 h. The product was extracted with chloroform and the organic phase was washed with 1M HCl, saturated NaHCO₃, water, and brine before being dried over MgSO₄. Finally, the solvent was removed in a rotatory evaporator, and the functionalization was checked by MALDI-TOF.

c. Synthesis of thermo-responsive ELR

The elastin-like recombinamer C₃(VPGVG)₈₄ was obtained using genetic-engineering techniques as described previously.^[S2] Briefly, it was produced using a 15 L bioreactor and subsequently was purified using the so-called Inverse Transition Cycling (ITC) process that consists in the repetition of several cycles of heating and cooling and exploiting the reversible LCST behavior of the ELR. The resulting product was characterized by several techniques such as HPLC, MALDI-TOF, and DSC in order to check their exact amino acid composition, molecular weight (Mw) as well as its LCST (Table S1, Fig. S5, S6)

d. Synthesis of Janus Au:Fe₃O₄ nanoparticles

The nanoparticle synthesis was performed as previously reported.^[S3] First, sphere-sphere heterodimers were synthesized in 1-octadecane (40 mL), oleic acid (6 mmol, 1.90 mL), oleylamine (6 mmol, 1.97 mL) and 1,2-hexadecanediol (10 mmol, 2.58 g) were added and stirred for 20 min at 140 °C under N₂. Fe(CO)₅ (1.5 mL) was then injected and after 3 min a solution containing HAuCl₄·3H₂O (0.1 mmol) dissolved in a mixture of oleylamine (0.5 mL) and 1-octadecane (5 mL) was injected and heated up to 310 °C at 1 °C min⁻¹. The solution was left to react for 45 min under mechanical stirring. After cooling down, the dispersion was exposed to air for 30 min to cause Fe oxidation. To purify the heterodimers, 50 mL of isopropanol was added and the solution centrifuged at 4500 g for 30 min. The nanoparticles were cleaned up two more times after redispersion

with hexane and aggregation with isopropanol. Finally, oleylamine (100 μL) was added to store the nanoparticles for long periods in a hexane–chloroform solution. The final nanoparticles had a diameter of: $d(\text{Fe}_3\text{O}_4) = 15.9 \pm 3.2 \text{ nm}$, $d(\text{Au}) = 6.0 \pm 1 \text{ nm}$.

To synthesize the Janus magnetic nanostars, the initial heterodimers that act as seeds were cleaned three times in ethanol and dispersed in chloroform to remove as much as oleylamine as possible. Then, they were dispersed in chloroform at a concentration of 2 mg mL^{-1} . A small quantity of carboxyl terminated PEG was added to the solution (to have approximately 2 mg/mL of polymer) and left for 1 hour. A solution of $\text{HAuCl}_4 \cdot 3\text{H}_2\text{O}$ (81.9 μL , 50 mM) was added to a freshly prepared solution containing polyvinylpyrrolidone (PVP) (0.75 g, $\text{MW} = 10 \text{ kg mol}^{-1}$) dissolved in DMF (15 mL). The solution was left stirring to allow gold salt prereduction from Au^{3+} to Au^+ (the reaction time is highly dependent on the PVP batch and needed to be adjusted by UV-Vis, in this case it was 5 min). The heterodimer nanoparticle solution was then quickly added and the reaction was left reacting for 1 h, showing a fast color change into blue. The amount of seeds added to the growth solution controls the final nanostar size, in this case 600 μL for nanoparticles (1) and 150 μL for nanoparticles (2). The nanoparticles were purified in 3 centrifugation cycles in DMF, and finally dispersed in 1 mL of DMF. The final nanostar equivalent diameter was 11 ± 2 and $23 \pm 3 \text{ nm}$ for nanoparticles (1) and (2) respectively.

The synthesized nanoparticles showed single-crystal Fe_3O_4 structure, with only a few cases with two single-crystal lobes, and a polycrystalline Au part with single-crystal tips, as previously reported^[S3] and in accordance with the synthesis of the different parts.^[S4,S6]

Complete characterization of nanoparticles, including HRTEM, electron tomography, XRD, XPS, VSM, ZFC/FC, magnetic relaxivity, reflectance spectroscopy, XANES, EXAFS, etc. can be read in the previous publications.^[S3, S6, S7]

e. Amphiphilic functionalization

The nanoparticle Au concentration was approximately obtained by assuming an absorbance of 1.2 at 400 nm corresponding to 0.5 mM.^[S9] Note that this was an overestimation due to the presence of iron oxide. The amount of thiol-terminated PS, calculated to be around 50 lig/nm² assuming a spherical Au, was dissolved in 50 μ L DMF solution. This was divided into aliquots and added in a stepwise procedure in 15 min intervals (see SI, figure S.2). The plasmon shift was monitored to determine the surface saturation. The red-shift was minimal after the addition of 50 μ L, however, most of the plasmon shift took place with the first 10 μ L. This last quantity was selected to functionalized the nanoparticles and avoid a high excess of the polymer in solution. The solution was left incubating for 2h and then the catechol-terminated PEG was added (100 lig/nm²) and left overnight to ensure a complete functionalization.

f. Amphiphilic self-assembly

1mL solution of nanoparticles (approximately 0.3 mM of Au) was placed on a glass cuvette with a small stirring bar. 111 μ L of water was slowly added under stirring, then the plasmon shift due to the self-assembly was monitored (see SI, figure S.3). After 2.5 h minimum change was observed. The nanoparticles were left for other 2 h and more water was added up to a ~70% water content. The assemblies were purified in water in a cellulose dialysis tubing (10 mm, cut-off 14000) for two days. 5 μ L of nanoparticle

solution was deposited on a previously glow-discharged carbon-coated grid and imaged by TEM.

For those nanoparticles containing long hydrophobic polystyrene (20 kg/mol), only 5% of water was enough to trigger the nanoparticle self-assembly. After leaving them overnight the assemblies were completely sedimented. The supernatant was exchanged by water and the assemblies were easily dispersed under stirring and after a few seconds in the sonication bath. The sedimentation and solvent exchange was performed a second time, and the final solution was used to prepare a TEM sample.

g. Thermo-responsive functionalization

A solution containing nanoparticles (2) was first centrifuged and dispersed in water. A solution containing ELR C₃(VPGVG)₈₄ at 50 lig/nm² was added and left to stir for 2 h. Then, a catechol-terminated PEG solution 100 lig/nm² was added and left overnight for complete functionalization. The nanoparticles were cleaned by centrifugation 3 times and dispersed in water. The final Au concentration was 0.33 mM. DLS and UV-Vis was used to characterize the thermal response of nanoparticles

h. TEM

TEM bright-field images were acquired in a JEOL JEM-1400PLUS instrument operating at 120 kV, after nanoparticles were deposited on a glow-discharged carbon-coated TEM grid. Nanoparticles were analyzed with the Image J software package. The nanoparticle equivalent diameter was taken from the area of the TEM 2D projection assuming a spherical shape. For the analysis of the number of nanoparticles per cluster (figure 2, C.1 and C.2) the nanoparticles were counted manually (number of clusters>300).

Tilt series for electron tomography were acquired in high angle annular dark-field scanning transmission electron microscopy mode on an aberration-corrected cubed FEI Titan electron microscope operated at 300 kV. The series was acquired within a tilt range from -76° to $+74^{\circ}$ and a tilt increment of 2° by using a Fischione model 2020 single-tilt tomography holder.

i. ICP

^{197}Au and ^{59}Fe were determined by iCAP-Q ICPMS (Thermo Scientific, Bremen, Germany) with an autosampler ASX-520 (Cetac Technologies Inc., NE, USA) and analyzed with the software package QtegraTM v2.6 (Thermo Scientific, Bremen, Germany). The quantification was based on at least 5 point external calibrations. Prior to analysis, the settings were optimized by infusion of TUNE B iCAP Q solution (Thermo Scientific, Bremen, Germany).

The analyses were carried out in KED mode using He as collision gas in order to reduce possible polyatomic interferences. All the samples were measured in triplicate using Yttrium 89 for Fe and Indium 115 for Au as an internal standard. Blank samples containing 2% HNO_3 / 0.5% HCl were infused before the calibration curve and wash samples (2% HNO_3 / 0.5% HCl) were also measured after calibration and between samples. Calibration samples were prepared at 100, 50, 25, 10, 5, 1, $\mu\text{g/L}$ in 2% HNO_3 / 0.5% HCl from a certified stock solution from Inorganic Ventures (Lakewood, NJ, USA).

The solution for ICPMS was prepared by adding aqua regia to a solution of nanoparticles (200 μL of aqua regia and 50 μL of the sample). After 30 min, water was added to a final volume of 3 mL. The solution was further diluted if needed.

The Au/Fe molar ratio was 0.52 and 1.92 for nanoparticles 1 and 2 respectively. The iron oxide phase was mainly Fe₃O₄ as previously determined.^[S3] This would correspond to a Au/Fe₃O₄ volume ratio of 0.36 and 1.31 for nanoparticles 1 and 2 respectively.

j. DLS

DLS measurements were carried out with a Zeta-Sizer Malvern Instrument in backscattering mode. All experiments were performed at a 173° scattering angle in 1 mL polystyrene cuvettes. Experiments with temperature variation were performed in a step-wise manner with 5 min stabilization time followed by three measurements. Z-average, cumulant diameters were taken as an average of the three measurements.

2. Supporting figures

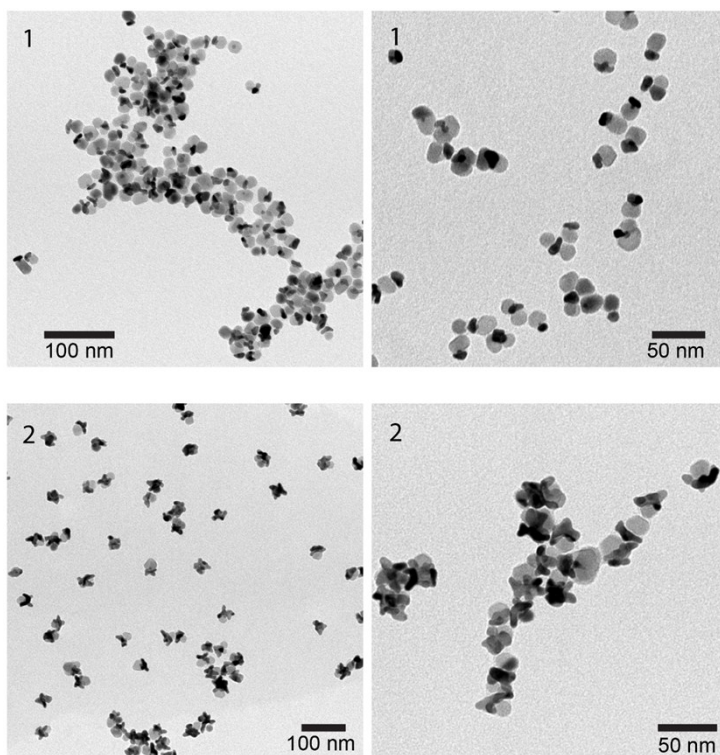


Figure S1. TEM images of Janus Au-nanostar/ Fe₃O₄ nanosphere of two different samples that share the same Fe₃O₄ lobes and two different Au nanostar sizes. Images 1 and 2 correspond to nanoparticles (1) and (2) of figure 1 respectively.

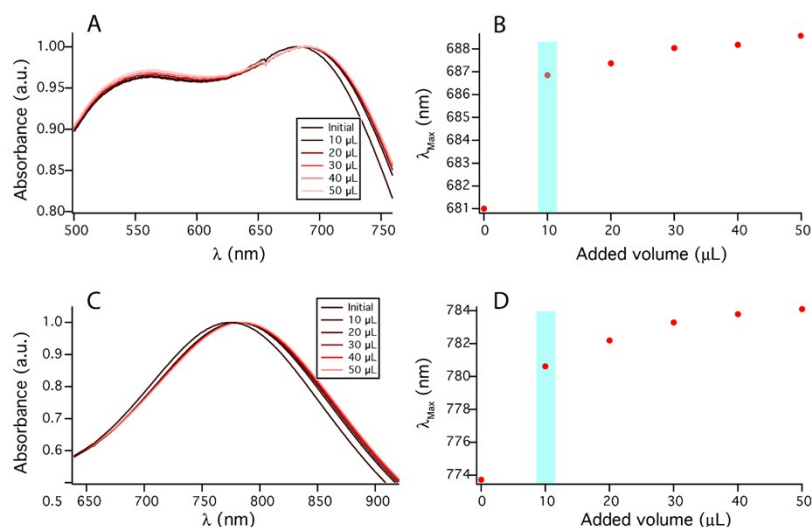


Figure S2. Functionalization of Janus nanoparticles with thiol-terminate polystyrene. A), C) UV-Vis spectrum of nanoparticles (1) and (2) respectively after normalization to the maximum absorbance. The different spectra correspond to the addition of a solution of thiol-terminated PS with 15 min intervals. The final total volume corresponds to approximately 50 lig/nm². B), D) Wavelength at maximum of figures (A) and (D) respectively. In blue it is marked the final amount of polymer selected for the functionalization, that guarantees good coverage and not much free extra polymer. Not much change was observed in the UV-Vis spectrum after overnight functionalization or inclusion of the PEG-catechol.

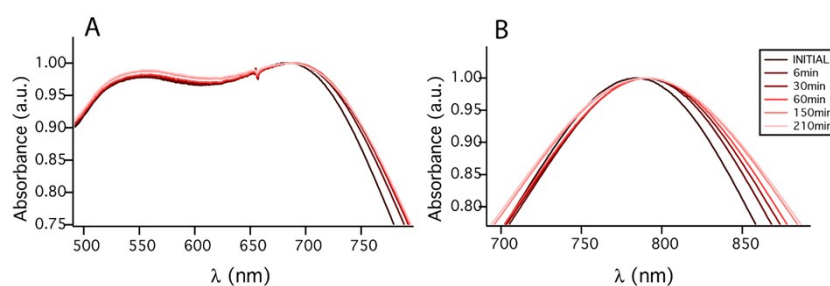


Figure S3. UV-Vis spectrum of Janus nanoparticle amphiphiles with short PS after the addition of 10% H₂O as a function of time. After 2 hours, the spectrum stabilized and there was no further plasmon shift.

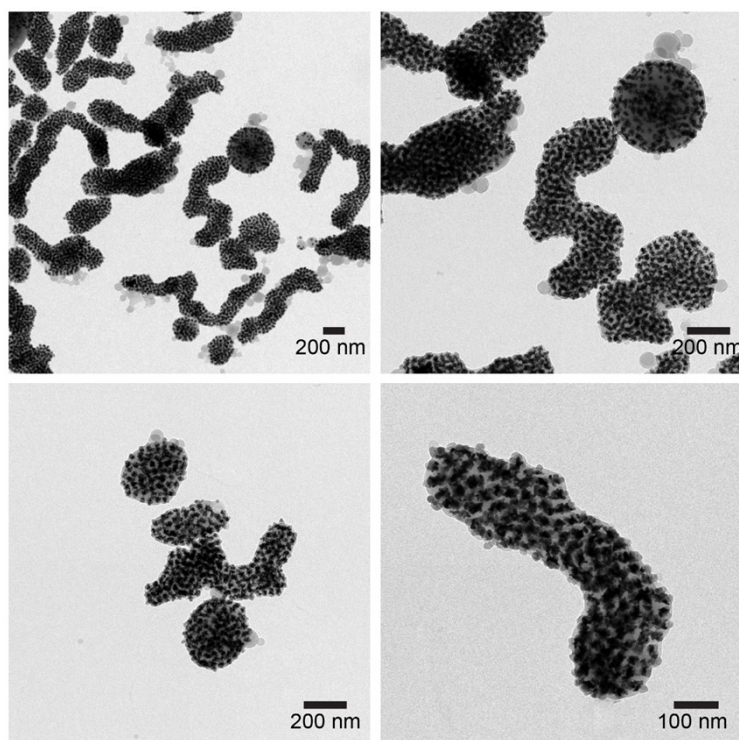


Figure S4. (A) TEM images of assemblies of nanoparticle amphiphiles (corresponding to nanoparticles of figure 1B1) with long PS (MW: 20 kg/mol).

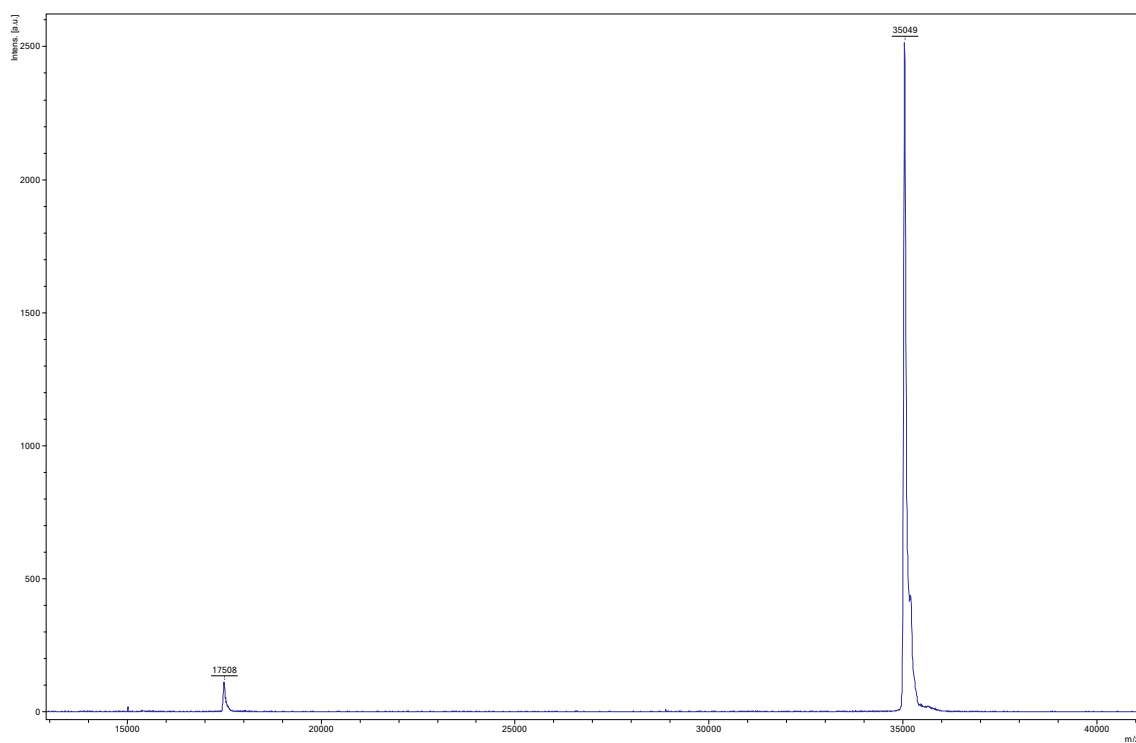


Figure S5. MALDI-TOF spectra of $C_3(VPGVG)_{84}$ -ELR. The two indicated peaks correspond to the singly and doubly charged ions respectively.

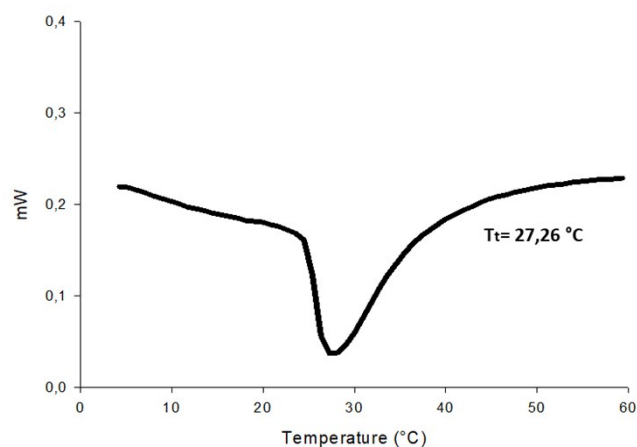


Figure S6. DSC graph showing the transition temperature of $C_3(VPGVG)_{84}$ -ELR at a concentration of 50 mg/mL in water.

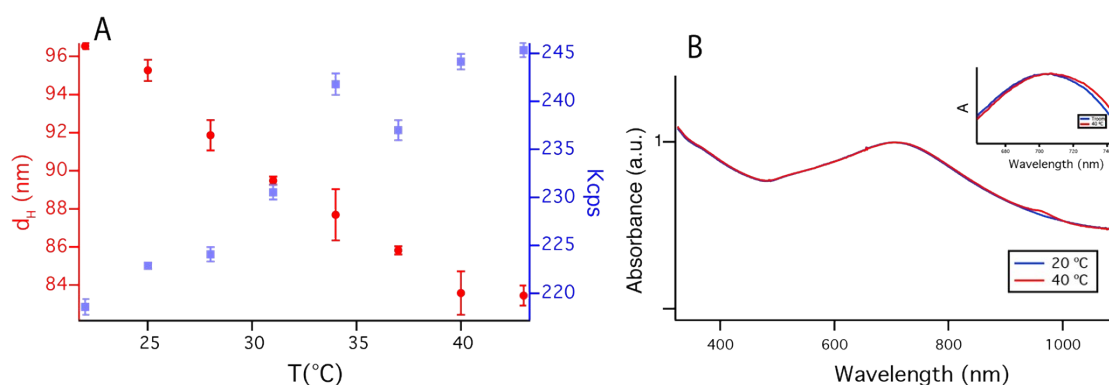


Figure S7. A) DLS of Janus thermo-responsive nanoparticles after functionalization and purification. Hydrodynamic diameter (red), and photon counting (blue) as a function of the temperature showing a shrinking and increase of refractive index of the thermo-responsive polymer that coats the Au part. B) UV-Vis of the nanoparticle solution showing a very small change in the absorbance spectrum from 20 to 40 °C. The inset shows a small shift of the plasmon band of ~3 nm.

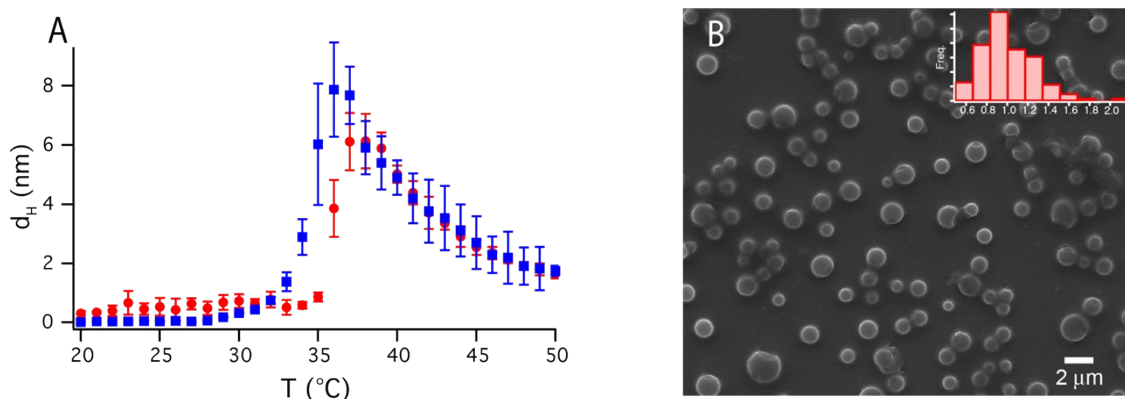


Figure S8. A) DLS of ELR solution with a concentration of 0.4 mg/mL. Cumulant hydrodynamic diameter (d_H) vs. temperature in a heating-cooling curve. B) SEM of ELR particles of micrometer size after heating, depositing on a Si wafer and freeze-drying process.

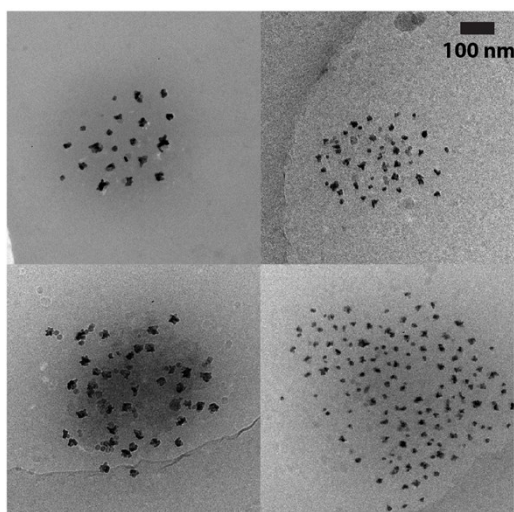


Figure S9. Cryo-TEM images of assemblies composed of an ELR polymeric core and stabilized by Au- Fe_3O_4 Janus switchable nanoparticle amphiphiles. [ELR] = 0.4 mg/mL.

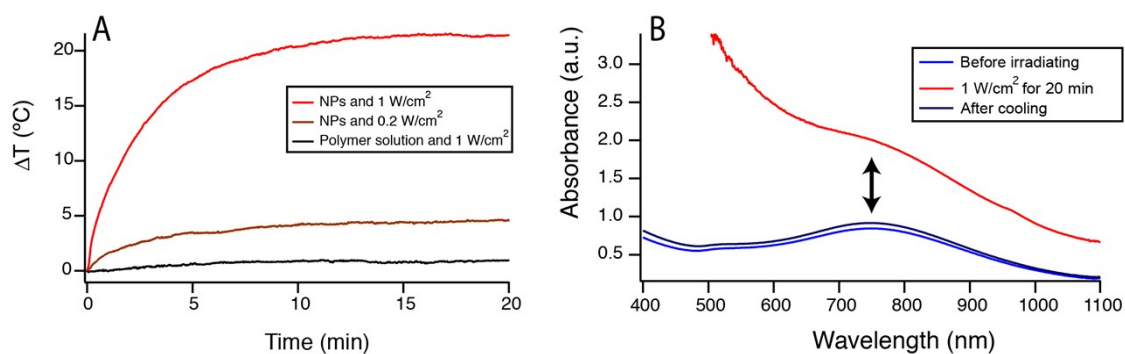


Figure S10. Light-triggered self-assembly of thermo-responsive Janus nanoparticles. A) Heating profile of a solution of thermo-responsive Janus nanoparticle containing 0.33 mM of Au and 1 mg/mL of ELR. 1mL of solution was placed in a glass cuvette 1x1x1 cm³ and irradiated laterally with 0.2 and 1 w/cm² with an 808 nm laser. As a control 1 mg/mL ELR water solution was irradiated at 1 W/cm². Temperature was measured from above using a thermographic camera. B) UV-Vis spectrum of the nanoparticle solution, the nanoparticle solution after irradiating with 1 W/cm² and the same solution after cooling down showing the reversibility of the system.

3. Supporting Tables

Table S1. Predicted and measured amino acid composition of C₃(VPGVG)₈₄-ELR

	PREDICTED	EXPERIMENTAL
G	176	178
C	3	2.89
V	177	177
M	1	0.99
P	84	84

4. References

- [S1] A. Klinkova, H. Therien-Aubin, R. M. Choueiri, M. Rubinstein, E. Kumacheva, *Proc. Natl. Acad. Sci. U.S.A.* **2013**, *110*, 18775–18779.
- [S2] J. C. Rodríguez-Cabello, A. Girotti, A. Ribeiro, F. J. Arias, in *Nanotechnology in Regenerative Medicine*, Humana Press, Totowa, NJ, **2012**, pp. 17–38.
- [S3] J. Reguera, D. Jiménez de Aberasturi, M. Henriksen-Lacey, J. Langer, A. Espinosa, B. Szczupak, C. Wilhelm, L. M. Liz-Marzán, *Nanoscale* **2017**, *9*, 9467–9480.
- [S4] H. Yu, M. Chen, P. M. Rice, S. X. Wang, R. L. White and S. H. Sun, *Nano Lett.*, 2005, *5*, 379–382.
- [S5] P. S. Kumar, I. Pastoriza-Santos, B. Rodríguez-González, F. de Abajo and L. M. Liz-Marzán, *Nanotechnology*, **2007**, *19*, 15606.
- [S6] S. Barbosa, A. Agrawal, L. Rodríguez-Lorenzo, I. Pastoriza-Santos, R. A. Alvarez-Puebla, A. Kornowski, H. Weller and L. M. Liz-Marzán, *Langmuir*, **2010**, *26*, 14943–14950.
- [S7] J. Reguera, D. Jiménez De Aberasturi, N. Winckelmans, J. Langer, S. Bals and L. M. Liz-Marzán, *Faraday Discuss.*, **2016**, *191*, 47–59.
- [S8] A. Espinosa, J. Reguera, A. Curcio, Á. Muñoz-noval, C. Kuttner, A. Van De Walle, L. M. Liz-marzán and C. Wilhelm, *Small*, **2020**, *16*, 1904960.
- [S9] T. Hendel, M. Wuthschick, F. Kettemann, A. Birnbaum, K. Rademann, J. Polte, *Anal. Chem.* **2014**, *86*, 11115–11124.